Applied Geochemistry 112 (2020) 104489

Contents lists available at ScienceDirect

Applied Geochemistry

journal homepage: http://www.elsevier.com/locate/apgeochem

Spatial and temporal variations of CO_2 emissions from the active fault zones in the capital area of China

Zhi Chen [a], Ying Li [a,*], Giovanni Martinelli [b], Zhaofei Liu [a], Chang Lu [a], Yuanxin Zhao [a]

[a] CEA Key Laboratory of Earthquake Prediction (Institute of Earthquake Forecasting), China Earthquake Administration, Beijing, 100036, China
[b] ARPAE Environmental Protection Agency of Emilia Romagna Region, 42100, Reggio Emilia, Italy

ARTICLE INFO

Editorial handling by Dr M Liotta

Keywords:
Geochemistry
Source of CO_2
Isotopic ratio
The capital of China
CO_2 concentration and flux

ABSTRACT

The chemical and isotopic composition of 26 soil gas wells and 11 springs along the active fault zones in the capital area of China was determined to investigate the origin of CO_2, the spatial and temporal variations of CO_2 emission, and their mechanisms. The chemical and isotopic data indicated that biogenic CO_2 was the primary source for CO_2 from the soil gas wells in both the basin and orogen regions, the crust-derived and mantle-derived CO_2 could have ascended through the deep-cut faults and got into the springs, with a few diffusing into the soil gas wells. Minor air could have intruded into the soil gas wells in the orogen region through the faults cutting the surface, owing to the barometric pressure fluctuation. Relatively high He concentration, CO_2 concentration, and flux of soil gas from wells were observed in the basin region than those in the orogen region. A significant amount of CO_2 is produced during the process of oxidation of organic matter in the basin, where the organic matter accumulates in thick clayey strata. Further amounts of CO_2 are produced by interactions between groundwaters and carbonates, which are widely represented in the basin region and by intruded air into the soil gas wells in the orogen region due to barometric pressure fluctuations. Temporal variations of CO_2 concentration and CO_2 flux were observed in soil gas wells in the basin region, where seismic activity is more frequent compared to those in the orogen, indicating that seismic activity could be responsible for the jumpily temporal variations of CO_2 concentration and flux in wells. Monitoring activities of soil gas CO_2 concentrations and CO_2 fluxes in active fault zones should be carried out.

1. Introduction

Earth degassing of CO_2 has been proven to contribute significantly to the global carbon budget (Camarda et al., 2009, 2016; Tamburello et al., 2018). Present-day investigation for earth degassing of CO_2 mainly focuses on volcanic, mud volcanic and geothermal regions (Chiodini et al., 1998; Etiope et al., 2007; Sun et al., 2017; Chen et al., 2019). However, volcano has been found to be the most relevant geologic body for earth degassing of CO_2, and investigation for spatial and temporal variations of soil CO_2 emission is identified as an essential tool for volcano activity monitoring, based on abundant researches (Irwin and Barnes, 1980; Pérez et al., 1996; Fu et al., 2005; Walia et al., 2010; Di Martino et al., 2013, 2016; Capasso et al., 2017; Camarda et al., 2019). While the investigation of nonvolcanic CO_2 discharges has risen exponentially in the last decades (Allard et al., 1991; Fu et al., 2005; Toutain et al., 2009; Caudron et al., 2012; Zhao et al., 2018).

Active faults and recent fractures are preferential migration pathways for deep gases (CO_2, Rn, He, etc.), due to their enhanced permeability and porosity relative to the surrounding rocks, along which gases can buoyantly migrate upwards (Doğăn et al., 2009; Fu et al., 2017; Chen et al., 2018, 2019). Recent investigations of origin and output of soil CO_2 degassing from active faults have been performed in locations that include China, America, Turkey, California etc. (Doğăn et al., 2009; Kulongoski et al., 2013; Lewicki et al., 2013; Jung et al., 2015; Zhou et al., 2016; Yuce et al., 2017), and high soil CO_2 concentration and flux have been frequently observed at active fault zones worldwide especially in extensional geological contexts (Chiodini et al., 2010; Han et al., 2014). The results of these studies suggest that CO_2 output from active faults can be of great importance to the global carbon budget (Italiano et al., 2009; Zhao et al., 2018). In addition, general overviews of the geochemical, structural, and seismic features in tectonically active areas have shown some evidence for the correlation between soil gas

* Corresponding author.
E-mail addresses: chenzhi@ief.ac.cn (Z. Chen), liying@ief.ac.cn (Y. Li), giovanni.martinelli15@gmail.com (G. Martinelli), liuzhaofei17@mails.ucas.ac.cn (Z. Liu), cealuchang@163.com (C. Lu), zhaoyuanxin18@mails.ucas.edu.cn (Y. Zhao).

https://doi.org/10.1016/j.apgeochem.2019.104489
Received 29 July 2019; Received in revised form 1 December 2019; Accepted 2 December 2019
Available online 5 December 2019

CO_2 anomalies and tectonic activities, and indicated that CO_2 discharge through faults and fractures in active fault zones might be enhanced by earthquake activity (Wakita et al., 1980; Toutain et al., 1992; Ciotoli et al., 1998; King et al., 1996; Italiano et al., 2009; Camarda et al., 2016; Sciarra and Coltorti, 2017). CO_2 concentration and flux surveys along active fault zones have been widely undertaken for researches oriented to contribute to earthquake forecasting (Caracausi et al., 2003; Fu et al., 2008; Sciarra and Coltorti, 2017). Investigations of the soil CO_2 concentration and flux from several active faults in the capital area of China have been carried out. The highest CO_2 concentration and flux were 9.5 vol % and 274.3 g m^{-2} d^{-1}, respectively. The total output of CO_2 from nine faults in the west of the capital area of China was 2.0 Mt, which was twice as that from the rupture zones produced by Wenchuan *Ms* 8.0 earthquake in western Sichuan, China (Li et al., 2013, 2018). Further information about CO_2 degassing and tectonic activities has been published by Sun et al. (2017), Wang et al. (2017), and Yang et al. (2018). Nevertheless, the origin of the soil gas CO_2, the spatial and temporal variations of CO_2 from the active faults in the capital area of China and their mechanism, are still unknown. In the present study, we at first time investigated the origins of CO_2 collected from the soil wells along the active faults in the capital area of China, analyzed the spatial and temporal variations of CO_2 degassing and their mechanism, and discussed the possible relation between soil gas CO_2 emission and tectonic activities.

2. Geological setting

The capital area is in the north of northern China and belongs to the Trans-North China Block and Eastern Block (Fig. 1). The tectonic setting in the area is complex, demarcated by the Taihangshan piedmont fault zone, the basin and range tectonics zone are distributed to the west, with the Bohai Bay basin to the east (Xu, 2002). In total, 21 active faults oriented in the NE-SW direction occur in the area, with 12 normal faults stretching to the west of Beijing, and the other nine strike-slip ones to the east. The study area is historically seismically active, 18 great earthquakes *($Ms > 6.0$)* have occurred in the area since 1618, for instance, the Sanhe-Pinggu earthquake ($Ms = 8.0$) in 1679 along the Xiadian fault zone, the Tangshan earthquake ($M_S = 7.8$) in 1976 along the Tangshan fault zone, followed by four aftershocks with magnitudes higher than 6.0. 11 hot springs with free gasses occur along the active fault zones in the capital area of China, the 6 ones in the orogen regions locate in effusive rocks and metamorphic rocks, and the others in the basin regions locate in the Quaternary sediments (Zhang et al., 2016; Li et al., 2018).

3. Methods

3.1. Gas measurement and sampling in the field

Based on the previous studies (Li et al., 2013, 2018; Sun et al., 2017; Wang et al., 2017; Yang et al., 2018), 26 sites were selected for soil gas well construction in November 2017 (Fig. 1) considering the following factors: (1) a location with higher CO_2 concentration than the background; (2) a location in the fault zone; and (3) a location with a distance exceeding 2.0 km from farmland, residential area and forest, to avert the effects due to microbial degradation of organic material and root respiration (Hoke et al., 2000; Gong et al., 2012; Tamir et al., 2012; Thomazini et al., 2016). Within one month after the site selection, construction of the soil gas wells was finished. An inverted PTFE circular accumulation hemispherical chamber with a volume of 1.7×10^{-2} m^3 and a radius of 0.2 m was fixed 5.0 m below the ground for each soil gas well. A 6-channel de-concentrator was installed on the inner wall of the chamber to re-inject the circulating gas in order to ensure the immediate and homogeneous mixture of gas in the chamber. Two exhaust tubes (PTFE, 5.0 m in length, 10 cm in diameter) were used, with their lower ends connected to the top of the chamber and their other ends connected to the inlet and outlet of the detector. This device formed a closed circuit for the soil gas (Fig. 2). Before CO_2 flux measurement, the chamber was purged by air injection through one of the two exhaust tubes, by an air pump with a flow rate of 15 L/min, meanwhile, continual monitoring for CO_2 concentration in the chamber was performed with the CO_2 monitor connected to the other tube, and the flux measurement was carried out until the CO_2 concentration in the chamber decreased to the atmospheric CO_2 concentration. Soil gas measurements were performed repeatedly in the field at the end of each month from July to November 2018 and April 2019. The CO_2 concentration and flux were measured by

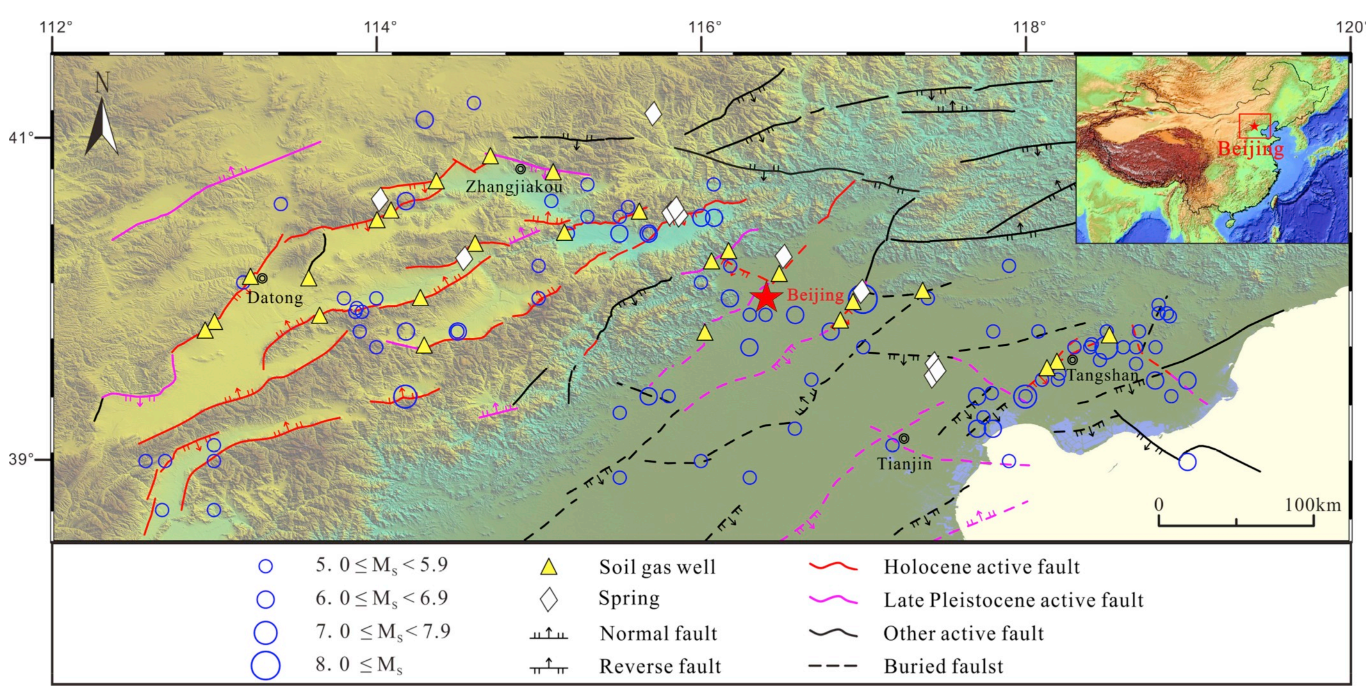

Fig. 1. Schematic geologic map of the research area.
Inset map shows the location of the studied region in China, the earthquakes are the events ($M_S \geq 5.0$) since 1618.

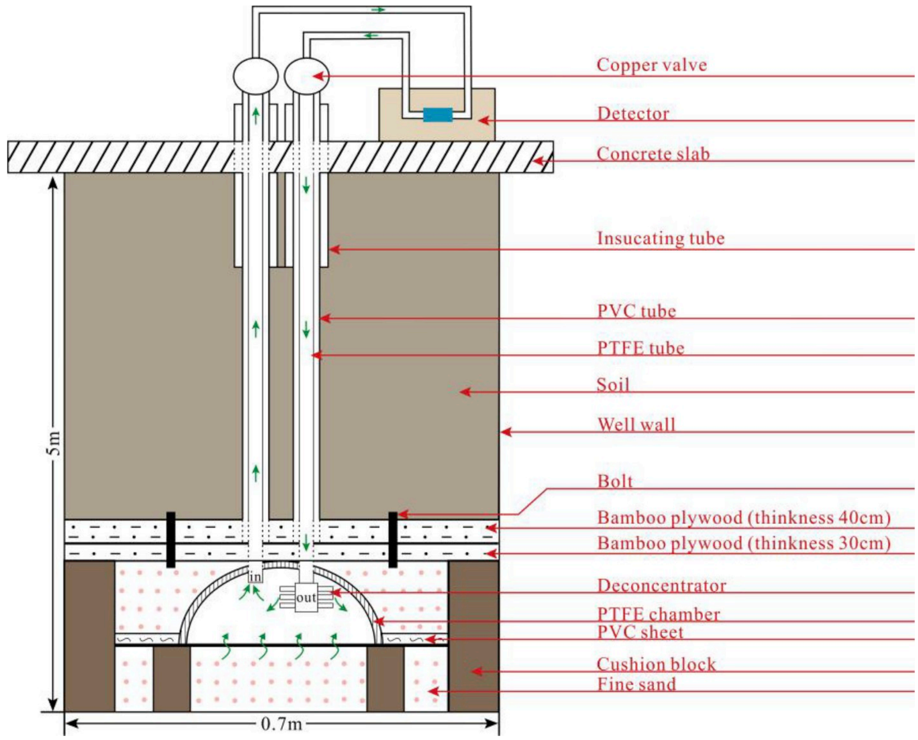

Fig. 2. Sketch of the constructed soil gas well.

a portable infrared CO_2 monitor (GXH-3010-E, for CO_2 concentration). The detection limit and measurement error of the GXH 3010-E CO_2 monitor was 0.01 vol % and ±2 vol %, respectively. An inlet filter was used to protect the detector from dust. The end connected to the outlet of the apparatus was plugged by a ball valve immediately after soil gas measurement.

Gas samples were collected by placing a cylindroid glass bottle (500 ml in volume, 0.5 cm in thickness, made of soda-lime glass) upside down. For the spring gas sampling, the glass bottle was pre-filled with spring water attained from each sampling site and connected with a rubber tube to an inverted funnel fully sunk in the spring (Zhang et al., 2016). For the soil-gas well sampling, the glass bottle was pre-filled with saturated brine and connected with a rubber tube to the outlet of the apparatus. Gas released from the springs and soil gas wells went through the tube and filled the soda-lime bottle by replacing the water inside, which was then sealed with solid trapezoidal rubber plugs and adhesive plaster on-site (Du et al., 2006; Dai et al., 2012). Three bottles of gas were collected in September 2018 and analyzed for He concentration and isotopic composition of CO_2 carbon, $\delta^{13}C_{CO2}$ (Chen et al., 2018).

3.2. Laboratory analysis

The He concentrations of soil gas were measured by an Agilent 3000 Micro GC with an error of ±5%. The carbon isotope $\delta^{13}C_{CO2}$ (V-PDB) values were determined by the MAT 253 plus stable isotope ratio mass spectrometer with uncertainties of ±0.3‰ in the Analytical Laboratory Beijing Research Institute of Uranium Geology. Analysis of all samples was completed within ten days of sampling.

4. Results

Twenty-six gas samples from the soil gas wells and 11 gas samples from the springs were collected in the field (Fig. 1). The CO_2 concentration and flux and their standard deviation, $\delta^{13}C_{CO2}$ (V-PDB), O_2 and He concentrations of gas samples from the soil gas wells were listed in Table S (Supplementary Material), and the CO_2 and He concentrations, $\delta^{13}C_{CO2}$(V-PDB), $^3He/^4He$ (R/Ra), Rc/Ra, He_M and $^4He/^{20}Ne$ of 11 spring gas samples were listed in Table 1.

The CO_2 concentration and flux obtained at the 26 soil gas wells were in the ranges of 0.1–11.4 vol % and 1.7–191.5 g m^{-2} d^{-1}, respectively, with the standard deviation ranging from 0.0 to 2.4 vol %, 1.0–44.7 g m^{-2} d^{-1}, respectively, the O_2 concentration and He concentration were in the range of 3.2–20.2 vol % and 4.9–11.5 ppm, respectively, and the $\delta^{13}C_{CO2}$ (V-PDB) varied from −20.9 to −18.0‰ (Table S).

The CO_2 and He concentrations of the 11 spring gas samples were in the ranges of 0.5–11.3 vol % and 574.0–4139.8 ppm, and the $\delta^{13}C_{CO2}$ (V-PDB), $^3He/^4He$ (R/Ra), Rc/Ra, $^4He/^{20}Ne$ were in the ranges of −15.6 ~ −8.9‰, 0.1–2.5, 0.1–2.5 and 17.8–185.5, respectively, the He_M was in the range of 1.0–31.4 vol% (Table 1).

R_C/Ra is the air-corrected $^3He/^4He$ ratio calculated using the method: $Rc/Ra = [(R/Ra \times X) - 1]/(X - 1)$, $X = [(^4He/^{20}Ne)_{measured}/(^4He/^{20}Ne)_{air}] \times \beta_{Ne}/\beta_{He}$. β is the Bunsen solubility coefficient, which is the volume of gas absorbed per volume of water at the measured temperature when the partial pressure of the gas is 1 atm (Weiss, 1971), assuming a recharge temperature of 15 °C. $\beta_{Ne}/\beta_{He} = 1.21$ at 15 °C. He_M is the mantle helium contribution of the total helium contents using the methods: $Rc/Ra = (R/Ra)_{crust} \times (1 - He_M) + (R/Ra)_{mantle} \times He_M$, $(R/Ra)_{mantle} = 8$ (Graham, 2002), $(R/Ra)_{crust} = 0.02$ (Andrews, 1985).

5. Discussion

5.1. Sources of CO_2 emitted from the soil gas wells

$\delta^{13}C_{CO2}$ (V-PDB) vs. $1/CO_2$, $^3He/^4He$ (R/Ra) vs. $^4He/^{20}Ne$ are regarded to be indicators for gas sources regions (Sano and Marty, 1995; Hernández et al., 2003; Doğăn et al., 2009; Yuce et al., 2017). Typical end-members for $\delta^{13}C_{CO2}$ of mantle and crust are −6.5‰ (vs. V-PDB) (Sano and Marty, 1995) and 0‰ (vs. V-PDB), respectively (Zhang et al., 2016), while for atmospheric and biogenic end members are −7‰ (vs. V-PDB) and −25‰ (vs. V-PDB), respectively (Dai, 1995; Doğăn et al., 2009). Typical end-members of $^3He/^4He$ for mantle, crust, and air are $1.1–1.4 \times 10^{-5}$, 2×10^{-8} and 1.4×10^{-6}, respectively (Ozima and

Table 1
Chemical and isotopic data of gas samples from the springs along the active fault zones in the Capital area of China.

Spring	CO_2 concentration (%)	δ^{13}_{CO2} (‰)	He (ppm)	R/Ra	Rc/Ra	He_M (%)	$^4He/^{20}Ne$
TZQ	0.6	−15.6	2075.1	0.4	0.4	5.0	85.4
JYWQ	3.5	−12.3	2288.4	2.5	2.5	31.4	96.1
YYBG	1.3	−13.9	2853.0	0.1	0.1	1.0	185.5
SSSZ	1.4	−13.8	1835.2	1.0	1.0	12.5	149.3
SSY	0.5	−11.9	718.4	2.4	2.4	30.1	63.2
WLY	1.0	−13.3	669.6	2.0	2.0	25.3	28.8
DYWQ	1.1	−11.2	1437.5	0.2	0.2	1.7	82.5
WSJ	11.3	−8.9	4139.8	0.5	0.5	5.9	44.5
DJWQ	7.7	−11.1	616.9	0.5	0.5	5.8	85.6
ZGST	1.7	−9.8	574.0	0.5	0.5	5.6	17.8
HSW	1.5	−11.2	673.8	0.5	0.5	6.5	20.7

R/Ra is the measured $^3He/^4He$ ratio in the samples divided by that of air (Ra = 1.4×10^{-6}).

Podosek, 1983), and those of $^4He/^{20}Ne$ for the mantle, crust and air are 1000, 1000 and 0.285, respectively (Hoke et al., 2000).

Fig. 3 shows as the He of the spring gases is a mixture of mantle and crust He with little air contamination for the spring gases, which could be taken as evidence for the presence of mantle-derived fluids entrained upward by the hydrologic system (Ballentine et al., 2002). Based on the simple crustal-mantle mixing model (Zhang et al., 2016), the mantle He contributions were calculated to be 1.0% ~ 31.4% (Table 1), while the crust the remaining. These spring gases could convey toward surface relevant signals from the deep earth. The P-wave velocity and S-wave velocity images indicate the existence of low-velocity bodies in the crust, accompanied by the uplift of the crust-mantle boundary and lateral variations of the upper mantle velocity structure, suggesting the upwelling and intrusion of upper mantle fluids (Huang and Zhao, 2004; Wang et al., 2009). The upper mantle fluids migrate upward through the faults along which the springs occur, and intrude into the springs (Doğăn et al., 2009; Fu et al., 2017), resulting in the high Rc/Ra (0.1–2.5) and $\delta^{13}C_{CO2}$ (V-PDB) (−15.6 ~ −8.9‰) values in the spring gases (Table 1).

In the $\delta^{13}C_{CO2}$ vs.$1/CO_2$ diagram, the soil gas samples and spring gas samples plotted within the composition mixing range between the Deep (M + C) end-member and biogenic end-member, while the soil gas samples plotted between the biogenic end-member and the spring gas samples (Fig. 4), this further indicate that the Deep (M + C) end-member and biogenic end-member should be the two potential CO_2 sources for both of the spring gas and soil gas, and the spring gas could be the secondary source for the soil gas, which played a role as the carrier of the deep volatile and transferred it to the shallower soil gas. CO_2 of the soil gas plotted closer to the biogenic end-member, which suggested that the

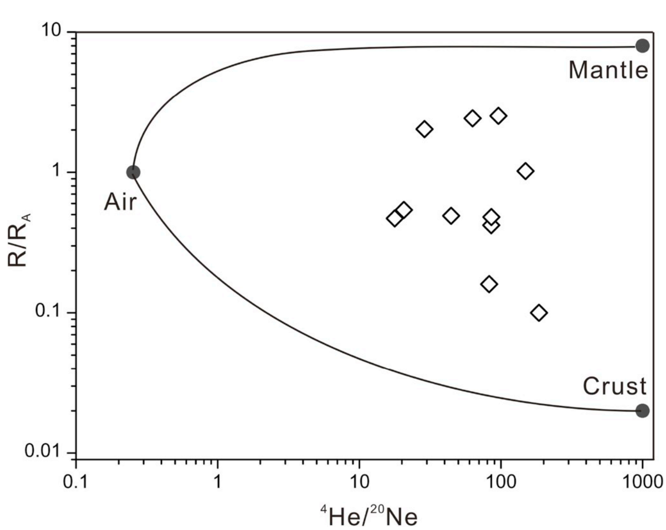

Fig. 3. Plots showing $^3He/^4He$ (Rc/Ra) vs. $^4He/^{20}Ne$ values for gas samples from the springs.

oxidation of organic matter during aerobic microbial respiration should have played the most important role in CO_2 production in the soil gas, and the concentrated distribution of the O_2 and CO_2 concentrations from the soil gas wells along the line (Y = - X) provided another further evidence (Fig. 5), and the process was represented as following (Romanak et al., 2012):

$$CH_2O + O_2 \rightarrow CO_2 + H_2O \quad (1)$$

Applying the $\delta^{13}C_{CO2}$ values for mantle (−6.5‰), crust (0‰) and biogenic (−25‰) end-members (Dai, 1995; Sano and Marty, 1995; Doğăn et al., 2009; Melián et al., 2014; Zhang et al., 2016), respectively, the biogenic CO_2 contributions for the spring gases were calculated to be between 12.0–62.4%, while for the soil gases to be in the range of 64.3–83.6%, which could suggest that mantle and crust CO_2 should be the main sources for the CO_2 from the spring gases, resulting in the higher $\delta^{13}C_{CO2}$ (−15.6 ~ −8.9‰) and He concentrations (574.0–4139.8 ppm), while biogenic CO_2 should be the main contributor to the CO_2 in the soil gases with lower $\delta^{13}C_{CO2}$ values (−20.9 ~ −18.0‰) and He concentrations (4.9–11.5 ppm) (Tables S and 1).

In addition, a noticeable difference was observed between CO_2 from the gas wells along the active faults in the orogen region and those in the basin region in the $\delta^{13}C_{CO2}$ vs.$1/CO_2$ diagram (Fig. 4), CO_2 from the soil gas wells in the basin region plotted along the mixing line between the biogenic end-member and deep (C + M) end-member, while those in the orogen region plotted along the mixing line between the biogenic end-member and air end-member, and with the O_2 concentrations deviating from the line (Y = - X) upward (Fig. 5), indicating the contamination of the air for CO_2 from the soil gas wells along the active faults in the orogen region. Most of the faults in the basin region along which the soil gas wells distributed are blind strike-slip faults lurking under the thick clay cover strata with the thickness up to 1000 m, while all of the faults in the orogen region are normal fault cutting the surface (Xu, 2002, 2015). Previous research indicated that the air could intrude into the earth through the high permeability fracture in the fault zone at a velocity of 10 m/d, subjecting to the barometric pressure fluctuation, with the largest depth up to 300 m (Auer et al., 1996; Illman and Neuman, 2001; Parker, 2003). Therefore, it could be inferred that the air had intruded into the soil gas wells in the orogen region through the faults that cut the surface, owing to the barometric pressure fluctuation, and resulting in the distinctive distribution of CO_2 along the mixing line between the biogenic end-member and air end-member in the $\delta^{13}C_{CO2}$ vs. $1/CO_2$ diagram (Fig. 4).

Based on the above results, the conceptual model for the sources and migration of CO_2 in the active fault zones in the capital area of China was summarized as that in Fig. 6. The crust-derived and mantle-derived fluids accumulating in the lower crust and upper mantle ascended through the deep-cut faults along which the springs occur, and intruded into the springs, while with minor crust-derived and mantle-derived gas diffusing into the soil gas wells. Although biogenic CO_2 was the main source for the soil gas wells in the study area, crust-derived and mantle-

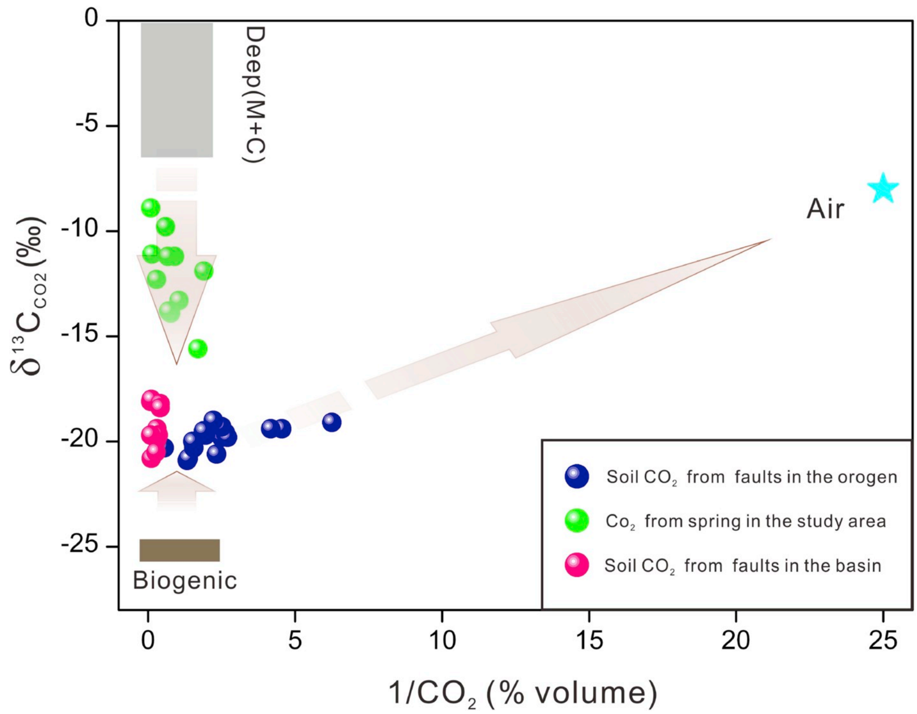

Fig. 4. Plot showing $\delta^{13}C_{CO2}$ vs.$1/CO_2$ values for gas samples from the soil gas wells and springs. Deep (M + C): end-member of mantle and crust sources, biogenic: end-member of biogenic source, Air: end-member of the atmospheric source.

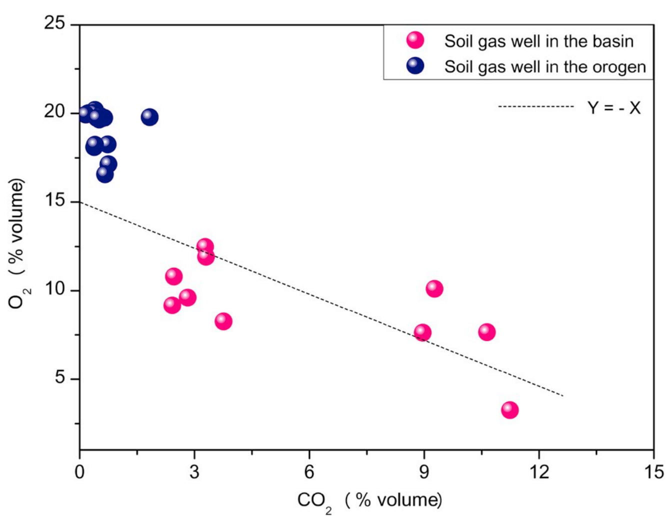

Fig. 5. Relationship between concentrations of O_2 and CO_2 from the soil gas wells.

derived CO_2 could be the secondary sources. In addition, the air should have intruded into the soil gas wells in the orogen region through the faults that cut the surface, owing to the barometric pressure fluctuation.

5.2. Variations of CO_2 emitted from the soil gas wells

5.2.1. Spatial variations of CO_2 emitted from the soil gas wells

Great spatial variation of CO_2 concentration and flux were observed in the soil gas wells along the active fault zones in the capital area of China (Fig. 7). High CO_2 concentration and flux were observed in the soil gas wells along the active fault zones in the basin region, with the concentration and flux in the range of 1.0–11.4 vol % and 16.3–191.5 g m^{-2} d^{-1}, respectively, which were much more higher than those in the orogen region, with the concentration and flux in the range of 0.1–1.8 vol % and 1.7–29.6 g m^{-2} d^{-1}, respectively, and the He concentrations were higher in the basin region too (Table S).

As being discussed above, the biogenic CO_2 was the main source for CO_2 from the soil gas wells along the fault zones in both the basin and orogen regions. In the O_2 concentrations vs. CO_2 concentrations diagram (Fig. 5), the gas samples from the soil gas wells in the basin region showed higher CO_2 concentration and lower O_2 concentration than those in the orogen region, which could indicate that more CO_2 should have been produced during the procedure of oxidation of organic matter during aerobic microbial respiration in the basin region, where the organic matter accumulates in the thick clay cover strata. Furthermore, carbonates are widely distributed in the geological formations (Xu, 2002; Feng, 2013; Yu et al., 2014), which should be another significant source for the CO_2 from the soil gas wells along the fault zones in the basin region, due to water-carbonate interaction, as Eq. (2) (Rovira and Vallejo, 2008; Tamir et al., 2011; Chen et al., 2015), while the air had intruded into the soil gas wells in the orogen region through the faults that cut the surface, owing to the barometric pressure fluctuation; these two factors should also take the responsibility for the great spatial variations of CO_2 concentration and flux observed between the CO_2 from the soil gas wells in the basin region and that in the orogen region. In addition, relative high He concentrations (9.2–11.5 ppm) were observed in the soil gas wells GLY, DDG, QXZ in the basin region, together with relative high CO_2 concentrations and fluxes (Table S, Fig. 7), which indicated the slightly more contribution of the Deep (M + C) end-member for the soil gas wells GLY, DDG, QXZ than others in the basin region. However, probably a low amount contribution of deep gas was not able to significantly change the $\delta^{13}C_{CO2}$, but it could accelerate the rate of CO_2 transport in the fault zone.

$$CaCO_3 + 2H^+ \leftrightarrow Ca^{2+} + CO_2(gas) + H_2O \quad (2)$$

5.2.2. Temporal variations of concentration and flux of CO_2 emitted from the soil gas wells

Temporal variations of soil gas CO_2 concentration and flux are primarily controlled by meteorological, biological and tectonic factors (Wood et al., 1993; Toutain and Baubron, 1999; Fu et al., 2017; Chen

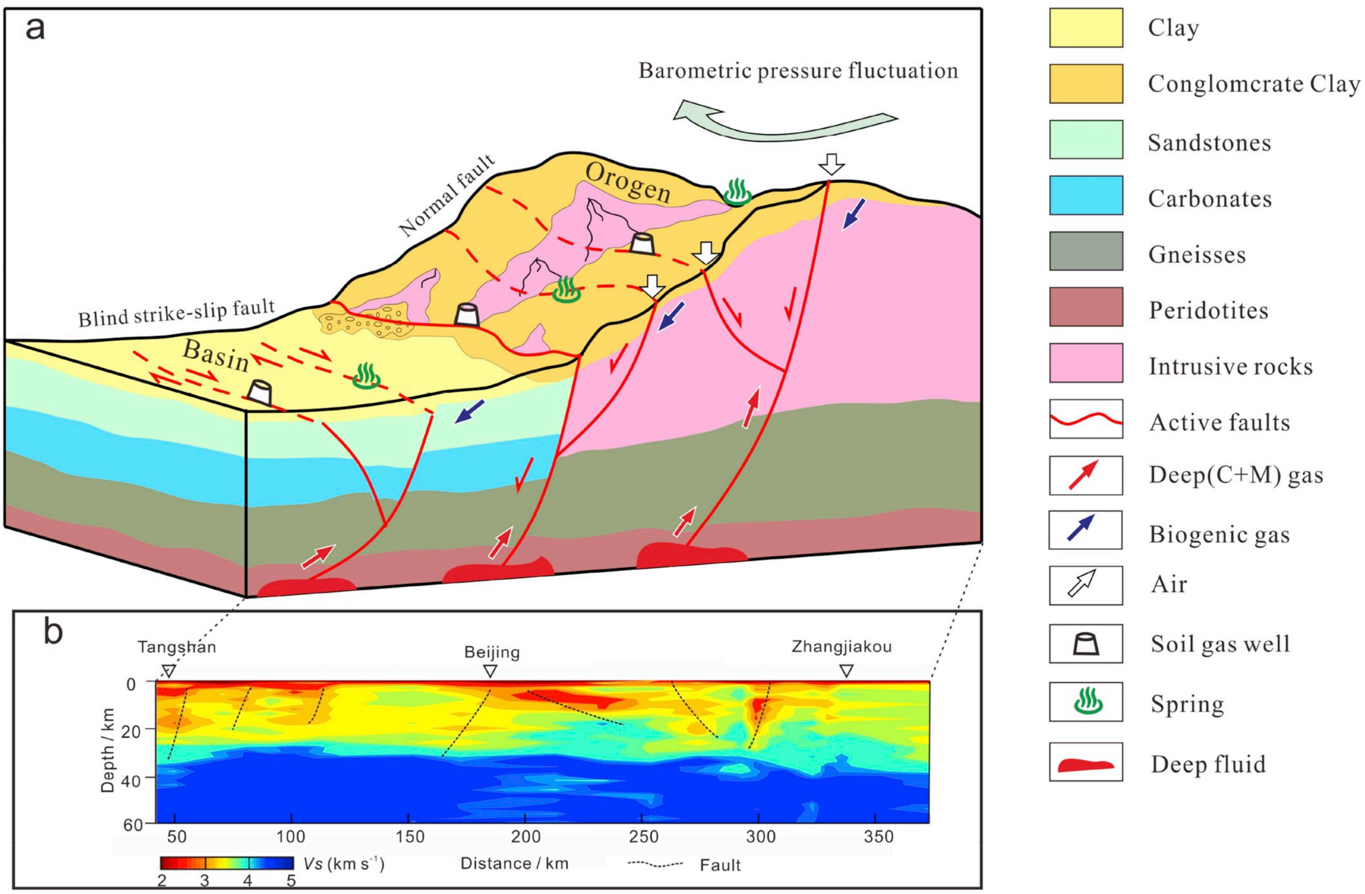

Fig. 6. A conceptual model for sources and migration of CO_2 in the active fault zones in the capital area of China.
(a) Conceptual model, (b) S wave velocity structure of the crust and mantle in the active fault zones in the capital area of China (Wang et al., 2009).

et al., 2019; Camarda et al., 2019). In our study, the CO_2 concentration and flux of the gas from the soil gas wells were observed in spring (April 2019), summer (July and August 2018), autumn (September and October 2018) and winter (November 2018) (Table S). However, the temporal variations of CO_2 concentration and flux could be random (Fig. 8), which were different from the regular seasonal variations (summer > autumn > winter > spring) proposed in the previous researches (Reardon et al., 1979; Greco and Baldocchi, 1996; Yakut et al., 2016). The capital area in the north of China is an arid and semi-arid area, the climate is characterized by long and cold winter with the absence of precipitation (Wei et al., 2008) (Fig. 8). Furthermore, to reduce the effect of meteorological and biological factors on soil CO_2 concentration and flux investigations, the chambers of the soil gas wells were fixed 5.0 m below the ground. At this depth, the seasonal effect on the biological activity and soil CO_2 had been proved to be negligible (Reardon et al., 1979; Wood et al., 1993), moreover, all of the soil gas wells were built far from the cropland and trees, therefore, the meteorological, biological factors should have little effect on the temporal variations of CO_2 concentration and flux in the soil gas wells in the active fault zones in the capital area of China.

In addition, the temporal variations of soil gas CO_2 concentration and flux showed significant differences between the soil gas wells in the basin region and those in the orogen region. Jumpily temporal variations of CO_2 concentration and flux were observed in the soil gas wells in the basin region, with the standard deviation for CO_2 concentration and flux in the range of 0.4–2.4 vol % and 5.8–44.7 g m^{-2} d^{-1}, respectively, while the temporal variations of soil gas CO_2 concentration and flux were slight in the orogen region, with the standard deviation for CO_2 concentration and flux in the range of 0.0–0.4 vol % and 1.0–6.3 g m^{-2} d^{-1}, respectively (Fig. 7), however, the meteorological parameters (atmospheric pressure, rainfall, and temperature) were similar for the orogen region and basin region (Fig. 9), which gave the further evidence for the insignificant impact of the meteorological, biological factors on the temporal variations of CO_2 concentration and flux in the soil gas wells in the active fault zones in the capital area of China, and the significant role of the tectonic factor had been highlighted inversely.

From July 2018 to April 2019, 17 earthquakes with magnitudes of 2.0–4.0 occurred in the study area (http://news.ceic.ac.cn), with 16 of the earthquakes occurred in the basin region, including 3 earthquakes with magnitudes of 3.0–3.9, and 14 earthquakes with magnitudes of 2.0–2.9, while only 1 earthquakes with magnitudes of 2.8 occurred in the orogen region (Fig. 7). It may be inferred that faulting activity is more effective in the basin region than in the orogen region, and that the more intense seismic activity could play an important role in the jumpily temporal variations of CO_2 concentration and flux in gas from the soil gas wells in the basin region. These degassing features can be found in a great part of geologic extensional contexts, as evidenced by Tamburello et al. (2018). Eventual fluctuation during time of deep originated CO_2 emission may be attributed to tectonic activity (e.g. Irwin and Barnes, 1980). Possible precursory characters of CO_2 degassing activity in extensional areas characterized by enhanced crustal permeability have been discussed by Martinelli and Dadomo (2017). Thus, this kind of geochemical prospection activities could be applied, in principle, in a great part of CO_2 degassing areas of the world. Therefore, the implementation of soil gas CO_2 concentrations and fluxes measurements in active fault zones for tectonic activity monitoring in researches oriented to possible earthquake forecasting could be envisaged.

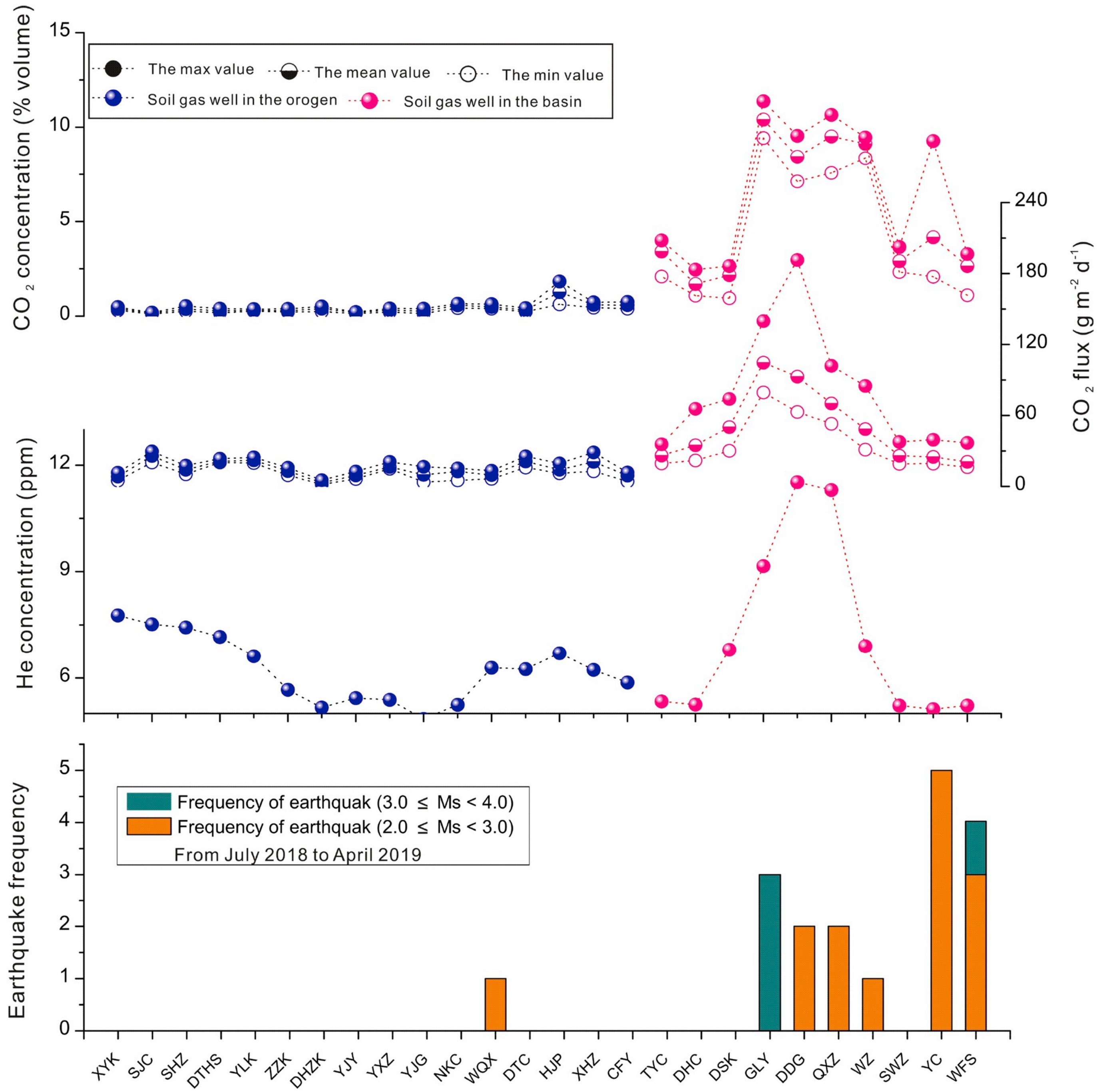

Fig. 7. Relationship between variations of He concentration, CO_2 concentration and flux in the soil gas wells and earthquakes.

6. Conclusions

Based on the chemical and isotopic characteristics of the collected gas samples from the soil gas wells and springs, the origin of CO_2 from the soil wells in the active fault zones in the capital area of China was analyzed, and the mechanisms for the spatial and temporal variations of CO_2 emission from the active fault zones were discussed.

The main conclusions are:

(1) The biogenic CO_2 is the primary source for the CO_2 from the soil gas wells in both the basin and orogen regions, a few crust-derived and mantle-derived CO_2 could have ascended through the deep-cut faults along which the springs occur, and diffused into the soil gas wells. Owing to the barometric pressure fluctuation, minor air should have intruded into the soil gas wells in the orogen region through the faults which cut the surface.

(2) The He concentration, CO_2 concentration and flux of soil gas from the wells in the basin region are much more higher than those in the orogen region, which can be attributed to the higher CO_2 amount produced during the process of oxidation of organic matter during aerobic microbial respiration in the basin region, where organic matter accumulates in the thick clay cover strata. Other two secondary CO_2 sources are represented by interactions between groundwaters and carbonates widely distributed in geological formations of the basin region and by air into the soil gas wells in the orogen region through the faults that cut the surface, due to the barometric pressure fluctuation.

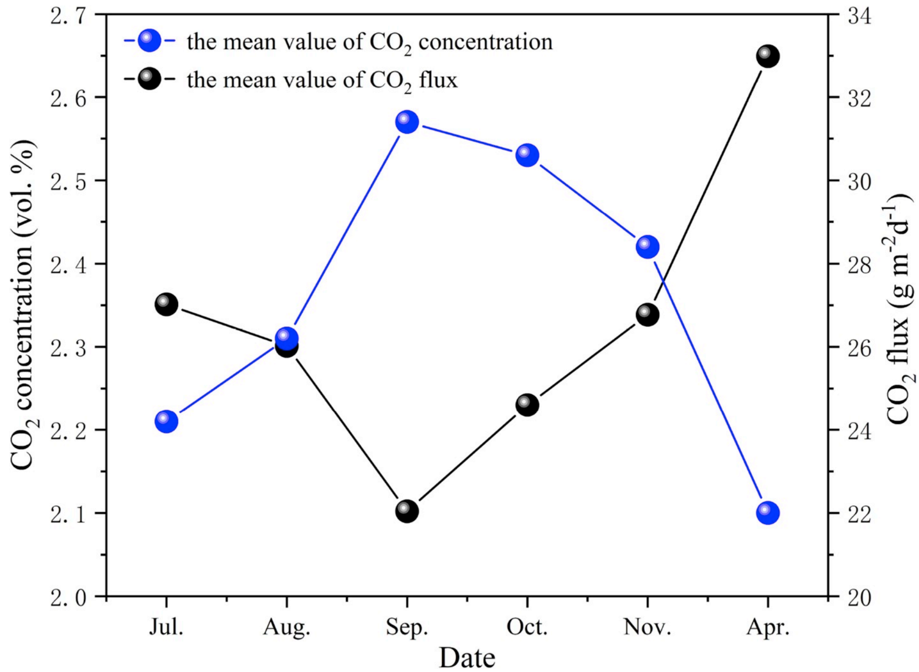

Fig. 8. Temporal variations of the mean values of CO_2 concentration and flux.

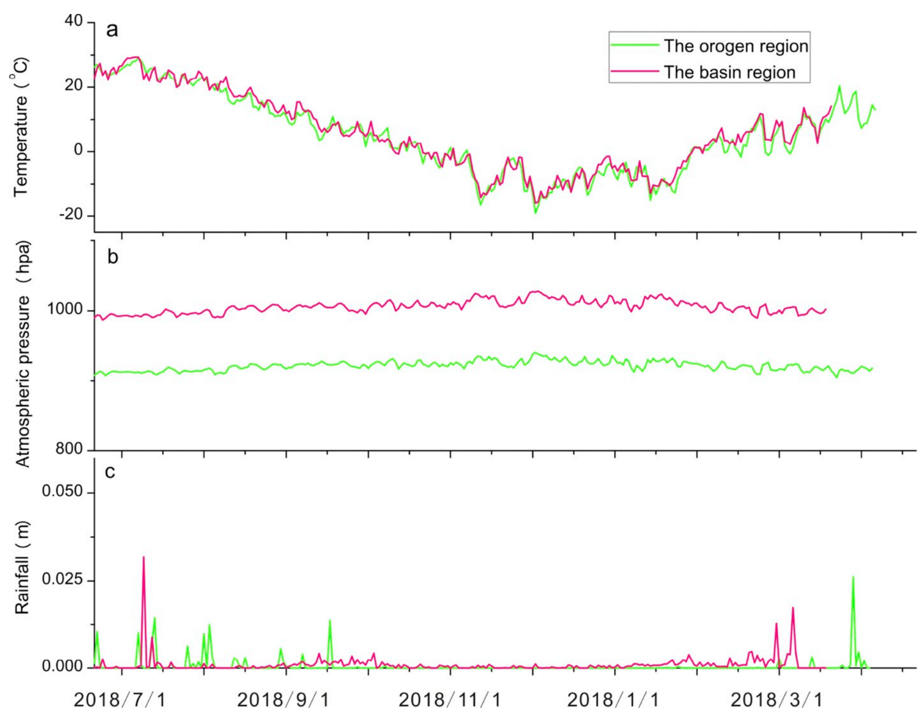

Fig. 9. Meteorological parameters (atmospheric pressure, rainfall, and temperature) in the capital area of China.

(3) Jumpily temporal variations of CO_2 concentration and flux were observed in the soil gas wells in the basin region, while the temporal variations of soil gas CO_2 concentration and flux were slight in the orogen region, which indicate that the more intense fault activity in the basin region than in the orogen region, and the more frequent seismic activity could play an important role in triggering the jumpily temporal variations of CO_2 concentration and flux in gas from the soil gas wells in the basin region. Therefore, the concentrations and fluxes of soil gas CO_2 in the active fault zones could be considered as preferential parameters for tectonic activity monitoring in researches oriented to possible earthquake forecasting.

Data availability statement

The data for this paper are available in the text.

Declaration of competing interest

The authors declare that they have no conflicts of interest.

Acknowledgements

The authors are grateful to Prof. Guodong Zheng and Liwu Li for analyzing the Gas compositions and isotopic data (Institute of Geology and Geophysics, Chinese Academy of Sciences). This study is jointly supported by the Basic Science Research Plan of the Institute of Earthquake Science, China Earthquake Administration (Nos. 2019IEF07032, 2016IES0102 and 20150112), the Natural Science Foundation of China (Nos. 41402298, 41573121 and 41503114).

Appendix A. Supplementary data

Supplementary data to this article can be found online at https://doi.org/10.1016/j.apgeochem.2019.104489.

References

Allard, P., Carbonnelle, J., Dajlevic, D., Bronec, J., Morel, P., Robe, M., Maurenas, J., Faivre-Pierret, R., Martin, D., Sabroux, J., Zettwoog, P., 1991. Eruptive and diffuse emissions of CO_2 from Mount EtnaJ. Nature 351, 387–391.
Andrews, J., 1985. The isotopic composition of radiogenic helium and its use to study groundwater movements in confined aquifers. Chem. Geol. 49, 339–351.
Auer, L., Rosenberg, N., Birdsell, K., Whitney, E., 1996. The effects of barometric pumping on contaminant transport. J. Contam. Hydrol. 24, 145–166.
Ballentine, C., Burgess, R., Marty, B., 2002. Tracing fluid origin, transport and interaction in the crust. Rev. Mineral. Geochem. 47, 539–614.
Caracausi, A., Favara, R., Giammanco, S., Italiano, F., Paonita, A., Pecoraino, G., Rizzo, A., Nuccio, P., 2003. Mount Etna: geochemical signals of magma ascent and unusually extensive plumbing system. Geophys. Res. Lett. 30 (2), 61–79.
Camarda, M., Gurrieri, S., Valenza, M., 2009. Effects of soil gas permeability and recirculation flux on soil CO_2 flux measurements performed using a closed dynamic accumulation chamber. Chem. Geol. 265 (3–4), 387–393.
Camarda, M., De Gregorio, S., Di Martino, R.M.R., Favara, R., 2016. Temporal and spatial correlations between soil CO_2 flux and crustal stress. J. Geophys. Res. Solid Earth 121. https://doi.org/10.1002/2016JB013297.
Camarda, M., De Gregorio, S., Capasso, G., Di Martino, R.M.R., Gurrieri, S., Prano, V., 2019. The monitoring of natural soil CO_2 emissions: issues and perspectives. Earth Sci. Rev. 198, 102928.
Capasso, G., Di Martino, R.M.R., Camarda, M., Prano, V., 2017. Dissolved carbon in groundwater versus gas emissions from the soil: the two sides of the same coin. Proc. Earth Planetary Sci. https://doi.org/10.1016/j.proeps.2016.12.021.
Chen, Z., Li, Y., Wang, C.G., Yan, L., 2015. Geochemical characteristics of water from mud volcano in the Wenquan county, Xinjiang. Earthq. Res. Sichuan 2, 12–15.
Caudron, C., Mazot, A., Bernard, A., 2012. Carbon dioxide dynamics in Kelud volcanic lake. Journal of Geophysical Research: Solid Earth 117 (B05102).
Chen, Z., Li, Y., Liu, Z., Wang, J., Zhou, X., Du, J., 2018. Radon emission from soil gases in the active fault zones in the Capital of China and its environmental effects. Sci. Rep. 8 (1), 16772.
Chen, Z., Li, Y., Liu, Z., Zheng, G., Xu, W., Yan, W., Yi, L., 2019. CH_4 and CO_2 emissions from mud volcanoes on the southern margin of the Junggar Basin, NW China: origin, output, and relation to regional tectonics. J. Geophys. Res.: Solid Earth 124. https://doi.org/10.1029/2018JB016822.
Chiodini, G., Cioni, R., Guidi, M., Marini, L., Raco, B., 1998. Soil CO_2 flux measurements in volcanics and geothermal areas. Appl. Geochem. 13, 543–552. https://doi.org/10.1016/S0883-2927(97)00076-0.
Chiodini, G., Granieri, D., Avino, R., Caliro, S., Costa, A., Minopoli, C., Vilardo, G., 2010. Non-volcanic CO_2 earth degassing: case of mefite d'Ansanto (southern apennines), Italy. Geophys. Res. Lett. 37 (11), L11303.
Ciotoli, G., Guerra, M., Lombardi, S., Vittori, E., 1998. Soil gas survey for tracing seismogenic faults: a case study in the Fucino Basin, central Italy. J. Geophys. Res. 103 (B10), 23781.
Dai, J., 1995. Abiogenic Gas in Oil-Gas Bearing Basin in China and its Reserviors. Natural Gas Industry.
Dai, J., Wu, X., Ni, Y., Wang, Z., Zhao, C., Wang, Z., Liu, G., 2012. Geochemical characteristics of natural gas from mud volcanoes in the southern Junggar Basin. Sci. China Earth Sci. 55, 355–367.
Di Martino, R.M.R., Camarda, M., Gurrieri, S., Valenza, M., 2013. Continuous monitoring of hydrogen and carbon dioxide at Mt Etna. Chem. Geol. 357, 41–51.
Di Martino, R.M.R., Capasso, G., Camarda, M., 2016. Spatial domain analysis of carbon dioxide from soils on Vulcano Island: implications for CO_2 output evaluation. Chem. Geol. 444, 59–70. https://doi.org/10.1016/j.chemgeo.2016.09.037.
Doğan, T., Sumino, H., Nagao, K., Notsu, K., Tuncer, M., Celik, C., 2009. Adjacent releases of mantle helium and soil CO_2 from active faults: observations from the Marmara region of the North Anatolian Fault zone, Turkey. Geochem. Geophys. Geosyst. 10 (11), 1–11.
Du, J., Cheng, W., Zhang, Y., Jie, C., Guan, Z., Liu, W., Bai, L., 2006. Helium and carbon isotopic compositions of thermal springs in earthquake zone of Sichuan, Southwestern China. J. Asian Earth Sci. 26 (5), 533–539.
Etiope, G., Martinelli, G., Caracausi, A., Italiano, F., 2007. Methane seeps and mud volcanoes in Italy: gas origin, fractionation and emission to the atmosphere. Geophys. Res. Lett 34 (L14303).
Feng, P., 2013. Tangshan Engineering Geological Layer Set in the Key Areas. Master thesis. Shijiazhuang University of economics, Hebei.
Fu, C., Yang, T., Lee, J., Walia, V., Liu, T., Lin, S., Chen, C., Hou, C., 2008. Variations of soil gases on the active Chihshang Fault in a plate suture zone, eastern Taiwan. Radiat. Meas. 44 (9), 940–944.
Fu, C., Yang, T., Chen, C., Lee, L., Wu, Y., Liu, T., Walia, V., Kumar, A., Lai, T., 2017. Spatial and temporal anomalies of soil gas in northern Taiwan and its tectonic and seismic implications. J. Asian Earth Sci. 149, 64–77.
Gong, W., Yan, X., Wang, J., 2012. The effect of chemical fertilizer on soil organic carbon renewal and CO_2 emission-a pot experiment with maize. Plant and Soil 353, 85–94.
Graham, 2002. Noble gas isotope geochemistry of mid-ocean ridge and ocean island basalts: characterization of mantle source reservoirs. Rev. Mineral. Geochem. 47, 481–538.
Greco, S., Baldocchi, D., 1996. Seasonal variations of CO_2 and water vapor exchange rates over a temperate deciduous forest. Glob. Chang. Biol. 2 (3), 183–197.
Fu, C., Yang, T., Walia, V., Chen, C., 2005. Reconnaissance of soil gas composition over the buried fault and fracture zone in Southern Taiwanand. Geochemical Journal 39, 427–439.
Han, X., Li, Y., Du, J., Zhou, X., Zhang, W., 2014. Soil gas Rn and CO_2 geochemistry across the active fault zones in the capital area of China. Nat. Hazards Earth Syst. Sci. 14, 2803–2815.
Hernández, P., Notsu, K., Tsurumi, M., 2003. Carbon dioxide emissions from soils at Hakkoda, north Japan. J. Geophys. Res. 108 (B4), 2210.
Hoke, L., Lamb, S., Hilton, D., Poreda, R., 2000. Southern limit of mantle-derived geothermal helium emissions in Tibet: implications for lithospheric structure. Earth Planet. Sci. Lett. 180, 297–308.
Huang, J., Zhao, D., 2004. Crustal heterogeneity and seismotectonics of the region around Beijing, China. Tectonophysics 385 (1–4), 159–180.
Irwin, W., Barnes, I., 1980. Tectonic relations of carbon dioxide discharges and earthquakes. J. Geophys. Res. Solid Earth 85 (B6), 3115–3121.
Illman, W., Neuman, S., 2001. Type curve interpretation of a cross-hole pneumatic injection test in unsaturated fractured tuff. Water Resour. Res. 37, 583–603.
Italiano, F., Bonfanti, P., Ditta, M., Petrini, R., Slejko, F., 2009. Helium and carbon isotopes in the dissolved gases of Friuli Region (NE Italy): geochemical evidence of CO_2 production and degassing over a seismically active area. Chem. Geol. 266, 76–85.
Jung, N., Han, W., Han, K., Park, E., 2015. Regional-scale advective, diffusive, and eruptive dynamics of CO_2 and brine leakage through faults and well bores. J. Geophys. Res.: Solid Earth 120, 3003–3025.
King, C., King, B., Evans, W., Zhang, W., 1996. Spatial radon anomalies on active faults in California. Appl. Geochem. 11 (4), 497–510.
Kulongoski, J., Hilton, D., Barry, P., Esser, B., 2013. Volatile fluxes through the big bend section of the san andreas fault, California: helium and carbon-dioxide systematics. Chem. Geol. 339, 92–102.
Lewicki, J., Hilley, G., Dobeck, L., McLing, T., Kennedy, B., Bill, M., Marino, B., 2013. Geologic CO_2 input into groundwater and the atmosphere, Soda Springs, ID, USA. Chem. Geol. 339, 61–70.
Li, Y., Du, J., Wang, X., Zhou, X., Xie, C., Cui, Y., 2013. Spatial variations of soil gas geochemistry in the Tangshan area of Northern China. Terr. Atmos. Ocean. Sci. 24 (3), 323–332.
Li, J., Chen, Z., Lu, L., Zhou, X., Li, Y., 2018. Degassing of CO_2, Rn and Hg from the Xiadian active fault and their environmental significance. Bull. Miner. Petrol. Geochem. 37 (4), 629–638.
Martinelli, G., Dadomo, A., 2017. Factors constraining the geographic distribution of earthquake geochemical and fluid-related precursors. Chem. Geol. 469, 176–184.
Melián, G., Hernández, P., Padrón, E., Pérez, N., Barrancos, J., Padilla, G., Dionis, S., Rodríguez, F., Calvo, D., Nolasco, D., 2014. Spatial and temporal variations of diffuse CO_2, degassing at El Hierro volcanic system: Relation to the 2011-2012 submarine eruption. Journal of Geophysical Research Solid Earth 119 (9), 6976–6991.
Ozima, M., Podosek, F., 1983. Noble Gas Geochemistry. Cambrige Univ. Pr.
Parker, J., 2003. Physical processes affecting natural depletion of volatile chemicals in soil and groundwater. Vadose Zone J. 2, 222–230.
Pérez, N., Wakita, H., Lolok, D., Patia, H., Talai, B., Mckee, C., 1996. Anomalous soil gas CO_2 concentrations and relation to seismic activity at Rabaul caldera, Papua New Guinea. Geogaceta 20, 1000–1003.
Reardon, E., Allison, G., Fritz, P., 1979. Seasonal chemical and isotopic variations of soil CO_2 at Trout Creek, Ontario. J. Hydrol. 43 (1), 355–371.
Romanak, K., Bennett, P., Yang, C., Hovorka, S., 2012. A process-based approach to CO_2 leakage detection by vadose zone gas monitoring at geologic CO_2 storage sites. Geophys. Res. Lett. 39, L15405.
Rovira, P., Vallejo, V., 2008. Changes in $\delta^{13}C$ composition of soil carbonates driven by organic matter decomposition in a Mediterranean climate: a field incubation experiment. Geoderma 144 (3), 517–534.
Sano, Y., Marty, B., 1995. Origin of carbon in fumarolic gas from island arcs. Chem. Geol. 119 (1–4), 265–274.
Sciarra, B., Coltorti, M., 2017. Learning from soil gas change and isotopic signatures during the 2012 Emilia seismic sequence. Sci. Rep. 7 (1), 14187.
Sun, Y., Zhou, X., Zheng, G., Li, J., Shi, H., Guo, Z., Du, J.G., 2017. Carbon monoxide degassing from seismic fault zones in the Basin and Range province, west of Beijing, China. J. Asian Earth Sci. 149, 41–48.
Tamir, G., Shenker, M., Heller, H., Bloom, P., Fine, P., Bartal, A., 2011. Can soil carbonate dissolution lead to overestimation of soil respiration? Soil Sci. Soc. Am. J. 75 (4), 1414.
Tamir, G., Shenker, M., Heller, H., Bloom, P.R., Fine, P., Bartal, A., 2012. Dissolution and recrystallization processes of active calcium carbonate in soil developed on tufa. Soil. Sci. Soc. Am. J. 76 (5), 1606.

Thomazini, A., Francelino, M., Pereira, A., Schünemann, A., Mendonça, E., Almeida, P., Schaefer, C., 2016. Geospatial variability of soil CO_2-C exchange in the main terrestrial ecosystems of Keller Peninsula, Maritime Antarctica. Sci. Total Environ. 2562, 802–811.
Toutain, J., Baubron, J., 1999. Gas geochemistry and seismotectonics: a review. Tectonophysics 304 (1), 1–27.
Toutain, J., Baubron, J., Bronec, J., Allard, P., Briole, P., Marty, B., Miele, G., Tedesco, D., Luongo, G., 1992. Continuous monitoring of distal gas emanations at Volcano southern Italy. Bull. Volcanol. 54, 147–155.
Toutain, J., Sortino, F., Baubron, J., Richon, O., Surono, S., Nonell, A., 2009. Structure and CO_2 budget of Merapi volcano during inter-eruptive periods. Bulletin of Volcanology 71, 815–826.
Wakita, H., Nakamura, Y., Kita, I., Fujii, N., Notsu, K., 1980. Hydrogen release: new indicator of fault activity. Science 210 (4466), 188–190.
Wang, J., Liu, Q., Chen, J., Li, S., Guo, S., Li, l., 2009. Three-dimensional S-wave velocity structure of the crust and upper mantle beneath the Capital Circle Region from receiver function inversion. Chin. J. Geophys. 52 (10), 2472–2482.
Wei, F., Xie, Y., Mann, M., 2008. Probabilistic trend of anomalous summer rainfall in Beijing: role of interdecadal variability. J. Geophys. Res. 113, D20106. https://doi.org/10.1029/2008JD010111.
Wang, X., Li, Y., Du, J., Chen, Z., Zhou, X., Li, X., Cui, Y., Wang, H., Zhang, Z., 2017. Geochemical characteristics of soil gases Rn, Hg and CO_2 and their genesis in the capital area of China. Acta Seismologica Sinica 39 (1), 85–101.
Weiss, R., 1971. Solubility of helium and neon in water and seawater. J. Chem. Eng. Data 16 (2), 235–241.
Wood, B., Keller, C., Johnstone, D., 1993. In situ measurement of microbial activity and controls on microbial CO_2 production in the unsaturated zone. Water Resour. Res. 29 (3), 647–659.
Xu, X., 2002. Latest Crustal Tectonic Change and Earthquakes in the Capital Area of China. Science Press, Beijing.
Yakut, H., Tabar, E., Yildirim, E., Zenginerler, Z., Ertugral, F., Demirci, N., 2016. Soil gas radon measurement around fault lines on the western section of the north anatolian fault zone in Turkey. Radiat. Prot. Dosim. 173 (4), 1–9.
Yang, Y., Li, Y., Guan, Z., Chen, Z., 2018. Correlations between the radon concentrations in soil gas and the activity of the Anninghe and the Zemuhe faults in Sichuan, southwestern of China. Appl. Geochem. 89, 23–33.
Yu, X., Yang, C., Dong, G., Zhan, D., 2014. Drilling and completion technology in the first geothermal well construction in Jixian system in Tangshan. Explor. Eng. Media 41 (2), 41–44.
Yuce, G., Fu, C., D'Alessandro, W., Gulbay, A., Lai, C., Bellomo, S., Yang, T., Italiano, F., Walia, V., 2017. Geochemical characteristics of soil radon and carbon dioxide within the Dead Sea fault and Karasu fault in the Amik basin (Hatay), Turkey. Chem. Geol. 469, 129–146.
Zhang, W., Du, J., Zhou, X., Wang, F., 2016. Mantle volatiles in spring gases in the Basin and Range Province on the west of Beijing, China: constraints from helium and carbon isotopes. J. Volcanol. Geotherm. Res. 309 (1), 45–52.
Zhao, J., Li, Y., Chen, Z., Liu, Z., Zhao, R., Rong, W., 2018. Correlation between gas geochemical emission and fault activity of the Yuxian-Guangling and Kouquan faults. Acta Seismologica Sinica 40 (6), 1402–1416.
Zhou, X., Chen, Z., Cui, Y., 2016. Environmental impact of CO_2, Rn, Hg degassing from the rupture zones produced by Wenchuan Ms 8.0 earthquake in western Sichuan, China. Environmental Geochemistry and Health 38 (5), 1067–1082.
Walia, V., Lin, J., Fu, C., Yang, F., Hong, W., Wen, L., Chen, C., 2010. Soil-gas monitoring: a tool for fault delineation studies along Hsinhua Fault (Tainan), Southern Taiwan. Applied Geochemistry 25 (4), 602–607, 2010.